Chebyshev Spectral-Collocation Analysis of Biomagnetic Au–Blood Nanofluid Flow and Heat Transfer over a Permeable Stretching Surface under Dipole Magnetic Actuation

Assyr Abdulle[1,*] and Bernard Louis Koff[2]

[1] Professor of Mathematics, EPFL; Mathematics Section, École Polytechnique Fédérale de Lausanne.
[2] Emeritus University Professor of Mathematical Sciences, Kent State University; adjunct professor at Case Western Reserve University.
* Correspondence: assyr.abdulle@epfl.ch

Abstract: The current research conducts an advanced high-order Chebyshev spectral collocation study of steady biomagnetic Au-blood nanofluid flow due to peristaltic movement of a linearly stretching plate with a localized magnetic dipole actuation effect. It accounts for the influences of wall suction, velocity slip, mixed convection, convective wall heating, viscous dissipation, Joule heating, and pyromagnetism. The blood is assumed to be the base liquid with gold nanoparticles added to the formulation via effective one-phase thermophysical properties accounting for the impact of nanoparticle inclusion on viscosity, density, specific heat, electrical conductivity, thermal conductivity, and thermal expansion. The problem is mathematically expressed in terms of coupled nonlinear partial differential equations. They are transformed into a corresponding system of ODEs, which are solved on Chebyshev–Gauss–Lobatto grid points, thus allowing exact calculation of wall gradient values for determination of the skin friction and heat transfer rates. The findings reveal that suction, slip effect, buoyant force, and larger Prandtl number accelerate hydrodynamic relaxation and suppress thermal penetration while the ferromagnetic interaction coefficient delays velocity development and elevates temperature due to the magnetization effect. Higher Biot and Eckert numbers intensify wall heat injection and enhance mechanical energy dissipation, respectively, leading to an increased thermal level. The present study reveals the interdependencies between the magnetic field, wall transpiration rate, and thermal effects that must be considered jointly when designing the wall response.

Keywords: biomagnetic fluid; gold–blood nanofluid; magnetic dipole; stretching sheet; spectral collocation; convective heat transfer; boundary-layer flow; biomedical transport

Citation: Assyr Abdulle and Bernard Louis Koff. 2021. Chebyshev Spectral-Collocation Analysis of Biomagnetic Au–Blood Nanofluid Flow and Heat Transfer over a Permeable Stretching Surface under Dipole Magnetic Actuation. *TK Techforum Journal (ThyssenKrupp Techforum)* 2021(2): 33–51.

Received: November-22-2020
Accepted: July-09-2021
Published: Sptember-30-2021

1. Introduction

Magnetic effects in fluid transport and heat exchange have become prominent in applied mechanics, thermal engineering, and bioengineering applications. Many modern technologies, including magnetic targeting of drugs, magnetic hyperthermia, blood purification, and lab-on-a-chip separations, rely on magnetic control of fluid motion and heating. Blood has particular potential in such systems because it is electrically conducting, slightly magnetizable, heat-sensitive, and exposed to steep fields at many medical devices. The boundary layer near high shear is amenable to description in the framework of the classical Newtonian fluid model in order to analyze the influence of magnetic forces, wall transpiration, and boundary conditions independently of other rheological effects [1–3].

This problem concerns biomagnetic fluid dynamics, which is characterized by two kinds of magnetic action on a fluid. Magnetohydrodynamic forces arise due to the interaction of current flowing in an electrically conducting fluid and external magnetic field. Ferrohydrodynamic forces result from magnetization gradient in a non-uniform field, whereas a non-zero magnetization can influence the thermal process. This distinction is

crucial for biomagnetic flow because of possible effects of localized fields on flow and thermal fields. The theoretical background of such problems includes ferrohydrodynamics and biomagnetics that deal with magnetic body forces acting on hydrodynamics and thermal processes via gradients of intensity and magnetization [4,5].

Magnetic dipole serves as a convenient way to localize the influence of magnetic forces. Unlike a constant transverse magnetic field, a dipole produces a strongly non-uniform field, whose intensity quickly diminishes far away from the source. Such a model can help analyze biomagnetic control in proximity of biomedical surfaces, microdevices, or magnetically actuated coatings. Biomagnetic flows induced by localized dipolar field have already been studied in some detail; previous works show that the field affects the wall shear stress and heat transfer rates. The present study employs the localized effect and combines it with a gold-blood nanofluid model in order to investigate thermal conductivity enhancement in combination with the action of the magnetic field.

As discussed above, heat transfer can be additionally affected by adding nanoparticles to the base fluid in order to obtain nanofluids. Since their conception, nanoparticles made of metal and oxides were considered, and it was demonstrated that nanofluids could increase the effective thermal conductivity and heat capacity without loss of continuum flow characteristics [6–8]. Nanoparticles made of gold are interesting for biomedical applications because of their high thermal conductivity, stability, photoactivity, and compatibility with sensing and treatment methods [9–11]. Adding gold nanoparticles to blood increases the effective thermal conductivity and heat capacity as well as other properties like viscosity and electrical conductivity. Consequently, nanoparticle content determines the strength of momentum diffusion, Joule heating, thermal diffusion, and buoyancy forces in nanofluid boundary layers.

Stretching surfaces are well known classical problems describing phenomena observed during polymer and sheet extrusion, metal rolling, and sheet coating. In the biomedical context, the stretching flow describes boundary-layer flows driven by walls of engineered biomedical devices [12–14]. Inclusion of transpiration, partial slip, and convective heating significantly enhances the physical relevance of such model, since all these mechanisms were found capable of changing wall shear stress and heat transfer rate [15–17]. Moreover, these effects are essential to construct a design-oriented magnetic model of biomagnetic transport.

Mixed convection and viscous dissipation can influence the thermal process as well. The former arises due to coupling of momentum and temperature equations, and the latter arises due to conversion of mechanical energy to thermal energy. In a nanofluid, these factors can be complicated by effective thermophysical properties and conversion of magnetic energy to heat. As a consequence, the wall heat transfer rate cannot be uniquely defined, and should be deduced based on magnetic field strength, suction and slip velocities, and wall boundary conditions [18–20].

It is clear that an adequate numerical procedure is needed in order to solve this problem because the equations are nonlinear, coupled, and involve high-order derivatives. Finite difference or shooting methods can yield qualitatively correct profiles, but engineering values require high accuracy of evaluation of boundary derivatives. Spectral Chebyshev collocation seems quite promising in this case because it possesses desirable features such as clustering of nodes at boundaries, efficient computation of high-order derivatives, and resolution of boundary-layer profiles with relatively small number of nodes [21–23]. Therefore, the spectral method is particularly useful for analyzing biomagnetic flows involving steep gradients and localized dipole term.

In this study, the goal is a physically meaningful and accurate solution of a boundary-layer problem involving a Au-blood nanofluid flow over a permeable surface under magnetic dipole actuation. A physically sound nanofluid model, similarity transformation, Chebyshev spectral method, benchmarking by validated heat transfer rate, and parametric analysis are used to reach the desired aims. Besides presentation of profiles and trends, the main objective here is understanding of the physical mechanism behind various effects

occurring in such boundary layers. This interpretation is essential for using the model as a guide for magnetically assisted biomedical transport and wall-controlled thermal management.

2. Physics and equations of motion

Consider steady two-dimensional laminar flow of a nanofluid with spherical gold particles over a linearly-stretching permeable plate. The coordinate system is placed such that the x axis lies along the plate while the y axis lies normal to it. Wall suction, velocity slip, and convection effects prevail on the wall of interest. A magnetic dipole exists beneath the stretching sheet and exerts a nonuniform magnetic field over the electrically-conducting fluid. Such a configuration constitutes a prototype of localized magnetic manipulation over a biomagnetic material surface [24]. The relevant physical situation is illustrated schematically in Figure 1.

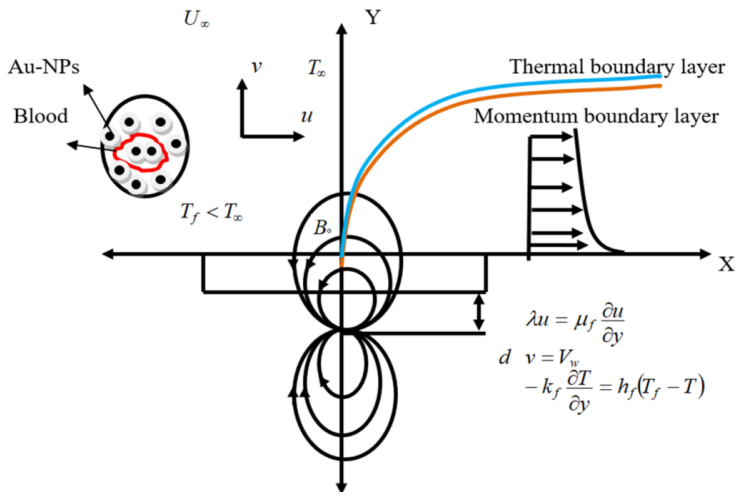

Figure 1. Physical geometry associated with the bio-magnetohydrodynamic Au–blood nanofluid flow over a permeable stretching sheet due to magnetic dipole actuation and convective heat flux exchange. This setup conforms with classical bio-magnetohydrodynamic modeling [1,4].

From Figure 1, it is observed that the wall serves as the point of tangential stretching, the wall suction controls the normal mass flow, and the dipole provides a nonuniform magnetic force acting beneath the boundary. As can be inferred, the physical geometry defined by the figure does not only depict boundary conditions but also signifies the three fundamental control parameters that dictate the results.

Assume stretching velocity distribution

$$U_\infty(x) = ax. \tag{1}$$

Here $a > 0$ represents the stretching rate of the sheet. Since this linear velocity formulation gives a fixed surface strain rate, self-similar solution is obtained for this case. Physically, higher values of a correspond to more rapid stretching, higher near-wall shear rate and hence thinner boundary layer thickness. Based on boundary-layer assumptions, the conservation equations for mass, momentum, and energy take the form [1,7]

$$\frac{\partial u}{\partial x}+\frac{\partial v}{\partial y}=0,$$

$$u\frac{\partial u}{\partial x}+v\frac{\partial u}{\partial y}=U_\infty\frac{dU_\infty}{dx}+\frac{\mu_{nf}}{\rho_{nf}}\frac{\partial^2 u}{\partial y^2}+g\beta_{nf}(T-T_\infty)-\frac{\sigma_{nf}B_0^2}{\rho_{nf}}(u-U_\infty)+\frac{\mu_0}{\rho_{nf}}M\frac{\partial H}{\partial x},$$

$$u\frac{\partial T}{\partial x}+v\frac{\partial T}{\partial y}+\frac{\mu_0 T}{(\rho C_p)_{nf}}\frac{\partial M}{\partial T}\left(u\frac{\partial H}{\partial x}+v\frac{\partial H}{\partial y}\right)=\frac{k_{nf}}{(\rho C_p)_{nf}}\frac{\partial^2 T}{\partial y^2}+\frac{\mu_{nf}}{(\rho C_p)_{nf}}\left(\frac{\partial u}{\partial y}\right)^2+\frac{\sigma_{nf}B_0^2}{(\rho C_p)_{nf}}(u-U_\infty)^2.$$

These are the equations used to provide mechanical and thermal equilibrium in the model. The continuity equation ensures that the system is incompressible, while the momentum equation maintains balance between stretching-induced inertia forces and viscous forces, buoyancy, Lorentz force, and magnetization gradient force. The energy equation maintains balance between convective forces, thermal diffusion, viscous heat dissipation, Joule heat dissipation, and energy dissipation due to the interaction between pyro-magnetism. It is significant where the magnetic terms are placed within the momentum and energy equations since the magnetic field affects the flow pattern as well as the dissipation of thermal energy.

The boundary conditions are specified as

$$\lambda u=\mu_f\frac{\partial u}{\partial y},\qquad v=V_w,\qquad -k_f\frac{\partial T}{\partial y}=h_f(T_f-T)\quad \text{at } y=0,$$

$$u\to U_\infty(x),\qquad T\to T_\infty\quad \text{as } y\to\infty.$$

The wall boundary conditions form three different engineering constraints. The slip flow velocity condition allows for finite tangential velocities at the surface while the suction condition enforces normal mass flux through the permeable sheet. The thermal convective condition allows for the possibility of changing wall temperature due to heat transfer between the wall and an external source of heat. The far-field boundary conditions impose that the fluid attains its free stream properties away from the boundary layer.

The gradient magnetic fields for the dipole field are taken to be as per [4,24]

$$\frac{\partial H}{\partial x}=\frac{\gamma}{2\pi}\left(-\frac{2x}{(y+d)^4}\right),\qquad \frac{\partial H}{\partial y}=\frac{\gamma}{2\pi}\left[-\frac{2}{(y+d)^3}+\frac{4x^2}{(y+d)^5}\right],$$

This peculiar dependence on $(y+d)^{-3}$ and $(y+d)^{-4}$ is associated with the local character of the dipole field. Thus, the dipole distance d controls the magnitude of the magnetic interaction in a proximity of the plate: small d means that the effect is concentrated near the wall, whereas large d implies an opposite behavior.

while magnetization is taken in the form of the linear pyromagnetic model,

$$M=K(T-T_f), \tag{2}$$

with K being the pyromagnetic constant. Such a relationship implies temperature-dependent magnetization, so the magnetic body force cannot be considered separately from the heat field. Hence, any change in temperature alters magnetic behavior, and vice versa, changes in the magnetic field affect energy balance through the coupled magneto-thermal effects.

2.1. Effective thermophysical properties

The Au–blood mixture is described as a one-phase nanofluid with the effective thermophysical characteristics calculated according to standard mixture equation [6]:

$$\begin{aligned}
\mu_{nf} &= \mu_f(1-\phi)^{-2.5},\\
(\rho C_p)_{nf} &= (1-\phi)(\rho C_p)_f + \phi(\rho C_p)_s,\\
\rho_{nf} &= (1-\phi)\rho_f + \phi\rho_s,\\
\beta_{nf} &= (1-\phi)\beta_f + \phi\beta_s,\\
\sigma_{nf} &= (1-\phi)\sigma_f + \phi\sigma_s,\\
\frac{k_{nf}}{k_f} &= \frac{(k_f+2k_s)-2\phi(k_f-k_s)}{(k_f+2k_s)+\phi(k_f-k_s)},
\end{aligned}$$

where ϕ is the nanoparticle volume fraction. These expressions show the influence of particle concentration on transport properties. The correction term in the Brinkman viscosity model increases resistance as ϕ increases, while the formula for thermal conductivity, according to the Maxwell theory, enhances the effective thermal conductivity due to the addition of a highly conducting solid to the base liquid. Moreover, the expressions for density, heat capacity, thermal expansion, and electrical conductivity describe the contribution of inertia, buoyancy, Joule effect, and heat accumulation to the dimensionless model equations. Such single-phase model is applicable to dilute and moderately loaded suspensions [25–27].

3. Similarity transformation

The transformation of the governing PDEs into an ODE system is achieved by introducing the similarity variables as [12,15,16]:

$$\eta = \sqrt{\frac{a}{\nu_f}}\,y, \qquad \psi = \sqrt{a\nu_f}\,x\,f(\eta), \qquad \theta(\eta) = \frac{T-T_\infty}{T_f-T_\infty},$$

where ψ is the stream function satisfying the continuity equation identically. The similarity variable η rescales the wall-normal distance by the viscous length associated with stretching, while θ converts the temperature field into a bounded dimensionless quantity. This transformation removes the explicit x-dependence from the boundary-layer equations and isolates the physical control parameters governing the flow.

$$u = \frac{\partial\psi}{\partial y}, \qquad v = -\frac{\partial\psi}{\partial x}.$$

These definitions ensure mass conservation before the momentum and energy equations are solved. They also show that the dimensionless function f contains both the streamwise velocity through f' and the wall-normal velocity through f, which is why suction enters the boundary condition on $f(0)$.

The transformed momentum and energy equations can be written in compact form as

$$f''' + A_1\left(ff'' - (f')^2 + 1\right) + A_2 Gr\,\theta - A_3 M(f'-1) - A_4\frac{2B\,\theta}{(\eta+\alpha)^3} = 0, \tag{3}$$

$$\theta'' + A_5 Pr\,f\theta' + A_6 PrEc\,(f'')^2 + A_7 MPrEc\,(f'-1)^2 - A_8\frac{2B\lambda_1 f(\varepsilon+\theta)}{(\eta+\alpha)^3} = 0, \tag{4}$$

Eq. (3) contains the dimensionless momentum balance. The first term is viscous diffusion, the nonlinear group $ff'' - (f')^2 + 1$ represents the stretching-flow inertial balance, $Gr\,\theta$ introduces buoyancy feedback from the thermal field, $M(f'-1)$ represents magnetic resistance relative to the free-stream stretching state, and the term proportional to $B/(\eta+$

$\alpha)^3$ captures localized dipole interaction. Eq. (4) contains the corresponding thermal balance. Thermal diffusion is opposed or supported by convective transport, viscous dissipation, Joule heating, and pyromagnetic energy exchange. These two equations therefore show explicitly why velocity and temperature cannot be interpreted independently in the present problem. subject to

$$f(0) = f_w, \qquad f'(0) = \beta f''(0), \qquad \theta'(0) = Bi\,[\theta(0) - 1], \tag{5}$$

$$f'(\infty) = 1, \qquad \theta(\infty) = 0. \tag{6}$$

The boundary conditions in Eqs. (5) and (6) translate the physical wall constraints into similarity form. The condition $f(0) = f_w$ fixes wall transpiration, $f'(0) = \beta f''(0)$ introduces partial slip through the wall shear, and $\theta'(0) = Bi[\theta(0) - 1]$ imposes conjugate convective heating. The far-field conditions close the boundary-value problem by requiring the velocity and temperature disturbances to vanish at large η.

The coefficient groups are defined by

$$\begin{aligned}
A_1 &= (1-\phi)^{2.5}\left(1-\phi+\phi\frac{\rho_s}{\rho_f}\right),\\
A_2 &= (1-\phi)^{2.5}\left(1-\phi+\phi\frac{\rho_s}{\rho_f}\right)\left(1-\phi+\phi\frac{\beta_s}{\beta_f}\right),\\
A_3 &= (1-\phi)^{2.5}\left(1-\phi+\phi\frac{\sigma_s}{\sigma_f}\right),\\
A_4 &= (1-\phi)^{2.5},\\
A_5 &= \frac{k_f}{k_{nf}\left(1-\phi+\phi\frac{(\rho C_p)_s}{(\rho C_p)_f}\right)},\\
A_6 &= \frac{k_f}{k_{nf}(1-\phi)^{2.5}},\\
A_7 &= \frac{k_f}{k_{nf}}\left(1-\phi+\phi\frac{\sigma_s}{\sigma_f}\right),\\
A_8 &= \frac{k_f}{k_{nf}}.
\end{aligned}$$

The controlling dimensionless parameters are

$$Pr = \frac{\mu_f C_{p,f}}{k_f}, \qquad Gr = \frac{\beta_f g(T_f - T_\infty)}{U_\infty a}, \qquad M = \frac{\sigma_f B_0^2}{\rho_f a},$$

$$Ec = \frac{U_\infty^2}{C_{p,f}(T_f - T_\infty)}, \qquad Bi = \frac{h_f}{k_f}\sqrt{\frac{\nu_f}{a}}, \qquad \alpha = \sqrt{\frac{a}{\nu_f}}\,d,$$

$$B = \frac{\gamma\mu_0 K(T_f - T_\infty)\rho_f}{2\pi\mu_f^2}, \qquad \beta = \frac{\mu_f}{\lambda}\sqrt{\frac{a}{\nu_f}}, \qquad f_w = \frac{-V_w}{\sqrt{a\nu_f}}.$$

It is these nondimensional groups that decide which physics is dominant in the boundary layer. While Pr is the ratio of momentum and thermal diffusivities, Gr compares buoyancy with stretching forces, M is a measure of Lorentz-type magnetic drag, Ec is a measure of energy transformation from mechanical to thermal, Bi is a measure of fluid-wall thermal interaction, B is a measure of dipole-induced magnetization interaction, β is the slip parameter, and f_w is the suction parameter.

3.1. Engineered quantities of interest

The wall shear stress and wall heat flux can be defined using skin friction coefficient and local Nusselt number as [16,17]

$$C_f = \frac{\tau_w}{\rho_f U_\infty^2}, \qquad Nu_x = \frac{x q_w}{k_f (T_f - T_\infty)},$$

The skin-friction coefficient represents the mechanical stress exerted on the sheet by the flow, while the Nusselt number captures the dimensionless heat transfer rate. In terms of practical significance, they can be considered as the most important outputs from a physical point of view since they directly relate the results to wall shear stress and heat dissipation at the wall. where

$$\tau_w = \mu_{nf} \left(\frac{\partial u}{\partial y} \right)_{y=0}, \qquad q_w = -k_{nf} \left(\frac{\partial T}{\partial y} \right)_{y=0}.$$

As seen from the above relations, it becomes clear that proper evaluation of wall values is of crucial importance. Having a graph which displays smooth variation of velocity or temperature profile is not sufficient; what counts are the wall slope values that indicate mechanical and heat transfer performance. After the use of similarity transformations, they become

$$Re_x^{1/2} C_f = \frac{1}{(1-\phi)^{2.5}} f''(0), \qquad Re_x^{-1/2} Nu_x = -\frac{k_{nf}}{k_f} \theta'(0).$$

From the similarity formulation, it is clearly seen that the wall value calculation is separated from the effective property correction factor in front of the derivatives. As seen from the above expressions, the presence of particles affects the shear stress coefficient through the viscosity factor, and the heat transfer rate through k_{nf}/k_f. Thus, behavior of both coefficients reveals boundary layer characteristics as well as fluid properties modification due to particle loading.

4. Spectral-collocation algorithm

The similarity equations stated in Eqs. (3)–(6) are solved using Chebyshev spectral collocation approach [21–23]. The semi-infinite domain is truncated to $0 \leq \eta \leq \eta_\infty$ such that η_∞ is sufficiently large so that the asymptotic boundary conditions are satisfied numerically. A linear transformation,

$$\eta = \frac{\eta_\infty}{2}(1 + \xi), \qquad -1 \leq \xi \leq 1,$$

The transformation changes the finite computation domain to the typical Chebyshev domain. Here, η_∞ has to be sufficiently large so that f' and θ have reached their asymptotic values, otherwise the far-field conditions used in the numerical computation will adversely affect the wall gradients. transforms the governing problem to the canonical domain.

The collocation points are set to be the Chebyshev–Gauss–Lobatto points,

$$\xi_j = \cos\left(\frac{j\pi}{N} \right), \qquad j = 0, 1, \ldots, N.$$

The concentration of the collocation points near $\xi = \pm 1$ is one of the reasons that make this method effective for solving boundary layer flow problems. As seen here, the wall region where the derivatives that are needed to calculate the skin friction coefficient C_f and heat transfer coefficient Nu_x are calculated receive more attention than the rest of the domain.

Suppose D is the differentiation matrix that corresponds to the first-order derivatives on these points, then the differentiation matrices for the physical domain are

$$D_\eta = \frac{2}{\eta_\infty} D, \qquad D_\eta^{(2)} = \left(\frac{2}{\eta_\infty}\right)^2 D^2, \qquad D_\eta^{(3)} = \left(\frac{2}{\eta_\infty}\right)^3 D^3.$$

Here, differentiation matrices are computed based on global polynomial representation of the unknowns. Since the momentum equation has f''' and the energy equation has θ'' as the highest order derivatives, the differentiation matrices are directly used instead of forming finite difference scheme.

Let the nodal vectors be written as

$$\mathbf{f} = [f(\eta_0), f(\eta_1), \ldots, f(\eta_N)]^T, \qquad \boldsymbol{\theta} = [\theta(\eta_0), \theta(\eta_1), \ldots, \theta(\eta_N)]^T.$$

The nodal vectors store the unknown values of velocity-potential and temperature functions at all collocation points. Once these values are known, every derivative appearing in the differential equations and in the wall quantities follows from matrix multiplication. At the interior nodes, the collocated residual equations become

$$D_\eta^{(3)}\mathbf{f} + A_1\Big(\mathbf{f} \odot D_\eta^{(2)}\mathbf{f} - (D_\eta \mathbf{f}) \odot (D_\eta \mathbf{f}) + \mathbf{1}\Big) + A_2 Gr\, \boldsymbol{\theta} - A_3 M(D_\eta \mathbf{f} - \mathbf{1}) - A_4 \mathbf{r}_1 \odot \boldsymbol{\theta} = \mathbf{0},$$
$$D_\eta^{(2)}\boldsymbol{\theta} + A_5 Pr\, \mathbf{f} \odot D_\eta \boldsymbol{\theta} + A_6 PrEc\, (D_\eta^{(2)}\mathbf{f}) \odot (D_\eta^{(2)}\mathbf{f}) + A_7 MPrEc\, (D_\eta \mathbf{f} - \mathbf{1}) \odot (D_\eta \mathbf{f} - \mathbf{1})$$
$$- A_8 \mathbf{r}_2 \odot \mathbf{f} \odot (\varepsilon \mathbf{1} + \boldsymbol{\theta}) = \mathbf{0},$$

This is the algebraic representation of the coupled boundary-value problem. The Hadamard products preserve the pointwise nonlinear interaction of convection, magnetic interaction, viscosity, and Joule heating. Thus, solution of the residual system leads to obtaining the full solutions for velocity and temperature distribution without any decoupling of hydrodynamics and heat transfer. where

$$\mathbf{r}_1 = \left[\frac{2B}{(\eta_j + \alpha)^3}\right]_{j=0}^{N}, \qquad \mathbf{r}_2 = \left[\frac{2B\lambda_1}{(\eta_j + \alpha)^3}\right]_{j=0}^{N},$$

and $\odot$ denotes the Hadamard product. The vectors $\mathbf{r}_1$ and $\mathbf{r}_2$ represent spatial decay of the effect of the dipole source within the interval of collocation nodes. Their maximum occurs near the wall, which corresponds to our physical expectations as the dipole effect should be strongest near the wall.

Newton iteration method is used to solve the system of nonlinear equations. The boundary conditions are fulfilled using row replacement of the residual and Jacobian matrices at each Newton iteration step such that the collocation conditions are met in the strong sense. Specifically, the calculations begin with some smooth profiles close to asymptotic far-field limits and iteratively solve the nonlinear system to make sure that the norms of residual and step are sufficiently small compared to the desired tolerance level. This approach is beneficial since the wall derivatives, which are needed for $f''(0)$ and $\theta'(0)$, can be found using the global approximation of the flow profile. This is an important feature of the method as the wall heat transfer coefficient and skin friction are much more sensitive to the numerical differentiation error than flow profiles [21–23].

5. Thermophysical properties and computational parameters

Thermophysical properties of blood and gold nanoparticles utilized in this study are given in Table 1. The selected values correspond to those widely reported in scientific literature [28–30]. The conductivity of gold is provided in the physically correct high-conductivity regime.

Table 1. Thermophysical properties of blood and gold nanoparticles used in Au–blood nanofluid model.

Property	Blood	Gold
Specific heat, C_p $(\mathrm{J\,kg^{-1}K^{-1}})$	3.9×10^3	129
Density, ρ $(\mathrm{kg\,m^{-3}})$	1050	19,300
Electrical conductivity, σ $(\mathrm{S\,m^{-1}})$	0.8	4.1×10^7
Thermal conductivity, k $(\mathrm{W\,m^{-1}K^{-1}})$	0.50	318
Thermal expansion coefficient, β $(\mathrm{K^{-1}})$	4.0×10^{-4}	1.4×10^{-5}

As can be seen from Table 1, there exists a marked difference between the physical properties of the blood and the gold materials. The gold material is characterized by higher density, higher electrical conductivity, higher thermal conductivity, and lower specific heat compared to blood. It means that even a small inclusion of particles will affect the magnetic property as well as the heat transfer rate; however, at the same time, it will make the fluid less sensitive due to increased viscosity.

The ranges of parameters for simulations of hydrodynamic and thermal fields are presented in Table 2. They are large enough to analyze the effect of magnetic forcing, dipole interactions, slippage, suction, buoyancy, convection, and viscous heating on the flow.

Table 2. Dimensionless parameter ranges employed in the spectral computations.

Parameter	Range or representative values
Prandtl number, Pr	17, 21, 25
Ferromagnetic interaction parameter, B	0 to 10
Nanoparticle volume fraction, ϕ	0.0, 0.001, 0.002, 0.02, 0.10
Dimensionless dipole distance, α	1.0
Magnetic parameter, M	1, 2, 3
Grashof number, Gr	1, 2, 3
Eckert number, Ec	1, 2, 3
Suction parameter, f_w	0.5, 1.0, 1.5
Slip parameter, β	0.5, 1.0, 1.5
Biot number, Bi	0.1, 0.3, 0.5, 0.7
Curie-temperature parameter, ε	78.5
Viscous-dissipation constant, λ_1	6.4×10^{-14}

The ranges chosen in Table 2 define the numerical space of parameters to be examined. The choice of parameters includes weakly up to stronger magnetic fields, moderate levels of convection heating, higher amounts of energy dissipation through viscosity, and realistic values for suction and slip phenomena. The use of very small to larger amounts of nanoparticles in the flow allows one to differentiate between a dilute biomaterial case and a more extreme alteration in the material properties.

6. Verification and Numerical Consistency

For a boundary layer solution, it is mandatory to show correctness of far field behavior, stability of the solution to changes in truncation boundary, and convergence of the wall data to increasing numbers of nodes [21,22]. In the current study, it is assured that the asymptotic conditions of $f'(\eta) \to 1$ and $\theta(\eta) \to 0$ are satisfied by taking the maximum value of η sufficiently large (η_∞). Then, the wall data for $f''(0)$ and $-\theta'(0)$ are checked for convergence with increasing node counts.

Table 3 [31] presents one example of quantative validation against published results for heat transfer coefficient for various values of Prandtl number and stretching exponent. It is clear that there is sufficient agreement to establish the correctness of the spectral method implementation. Furthermore, Fig. 2 depicts the expected velocity and temperature profiles at baseline conditions for a non-ferromagnetic fluid. Together, these checks establish that

the spectral scheme preserves the structure of the coupled transport problem and can be used confidently for parameter studies.

Table 3. Comparison of the local heat-transfer quantity $-\theta'(0)$ for selected values of n and Pr.

Pr	n	Reference result	Present result	Absolute error (%)
1	0.2	0.610262	0.610112	0.0246
1	0.5	0.595277	0.595863	0.0984
1	1.5	0.574537	0.574898	0.0629
5	0.2	0.607175	0.607160	0.0024
5	0.5	1.586744	1.607160	1.2869
5	1.5	1.557413	1.557214	0.0128

It can be seen from the minor differences in Table 3 that the spectral algorithm successfully mimics the baseline heat transfer rate over various combinations of Prandtl number and stretching index. This is particularly important since such a test allows checking the wall temperature gradient, which is more susceptible to numerical differentiation.

Figure 2 provides further proof of successful validation by illustrating how the shape of the velocity and temperature profile remains as expected. The accuracy of not only the form but also the behavior at the wall for both variables indicates the appropriateness of the used method for further parameter studies.

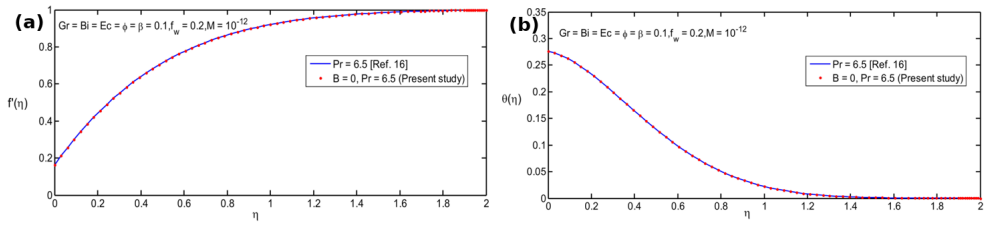

Figure 2. Verification of Chebyshev spectral-collocation method for the base case: computation and validation of (a) velocity profile $f'(\eta)$ and (b) temperature profile $\theta(\eta)$ with reference data from [31].

7. Results and discussion

The numerical findings explain how magnetic effects, wall control, and thermal conditions coordinate the Au–blood boundary layer. The key to interpreting the results lies in recognizing how each parameter changes the momentum equation or energy balance or interacts between the two through coupling. It matters which one of these three classes the parameter falls under since two flow situations with similar velocity distributions can differ in the rate of heat transfer by the wall, and two situations with similar temperatures can differ in wall shear if the momentum equation is modified by magnetic forces or slip. The rest of the discussion will relate the figures and tables to the specific physical mechanisms behind them.

7.1. Effect of wall suction and velocity slip

The variation in velocity and temperature caused by suction and slip is shown in Fig. 3. An increase in the suction parameter f_w decreases the amount of near-wall flow and shrinks both the hydrodynamic boundary layer and the thermal boundary layer. In dimensional variables, the flow field converges faster towards the free stream value, and the temperature distribution drops more rapidly outside the wall vicinity. Such results confirm the known ability of wall suction to stabilize and regulate the temperature boundary layer [13,16,17]. Engineering-wise, suction means the active management of walls: thermal accumulation at the interface is minimized by decreasing the residence time of the heated fluid particles, while the wall-normal gradients, critical for shear and heat exchange, are strengthened.

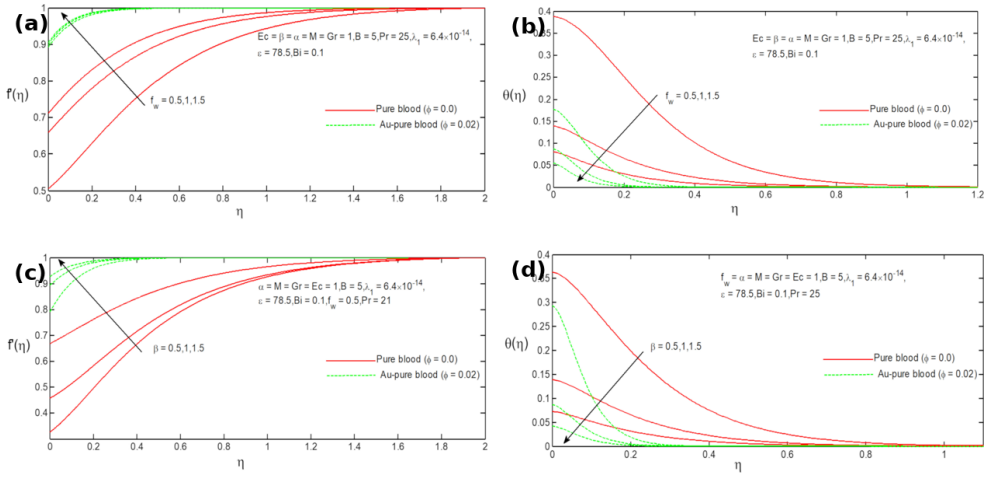

Figure 3. Computed influence of wall suction and velocity slip on the boundary-layer fields: (a) effect of f_w on $f'(\eta)$, (b) effect of f_w on $\theta(\eta)$, (c) effect of β on $f'(\eta)$, and (d) effect of β on $\theta(\eta)$. These trends indicate that suction shrinks boundary layers, while slip modifies near-wall momentum transport.

The opposite phenomenon occurs if the velocity slip parameter β rises. The closer fluid is no longer constrained by the rigid-wall condition, so its velocity profile becomes flatter in response. In turn, the heat transfer process becomes less effective since the near-wall flow now moves with lower wall shear. Slip may occur in a biofluid channel due to the presence of coated walls or structured surfaces. The present study demonstrates that moderate slip can affect the velocity profile and the efficiency of heat exchange, so the slip condition must be accounted for when analyzing biomagnetic flows in the vicinity of walls [14,15].

As seen from the four graphs in Figure 3, wall control influences the two boundary-layer functions in a slightly different way. Suction enhances both velocity and thermal gradients due to layer shrinking. The larger the slip, the smaller the shear at the wall becomes; however, increased slip can still lead to thinner thermal layers because near-wall mixing improves. Therefore, wall suction and velocity slip must be considered independent parameters because suction controls wall-normal mass flux, whereas slip manages wall shear.

7.2. Impact of dipolar effect and magnetic driving

In Figure 4, the role of the ferromagnetic interaction parameter B is examined. As noted, larger values of B reduce velocity profile height and elevate the temperature distribution in the boundary layer. This is consistent with a strong localized magnetic field leading to a larger magnetization-related body force and thermal perturbation due to the dipolar term in the energy equation. The retardation of momentum transfer increases the residence time of the fluid within the heated domain, offering a partial explanation for the thermal enhancement. It is relevant for biothermal engineering in terms of how localized magnetic forcing can influence not only particles' trajectories or flow resistance but also the thermal environment for the carrier fluid [4,5,32].

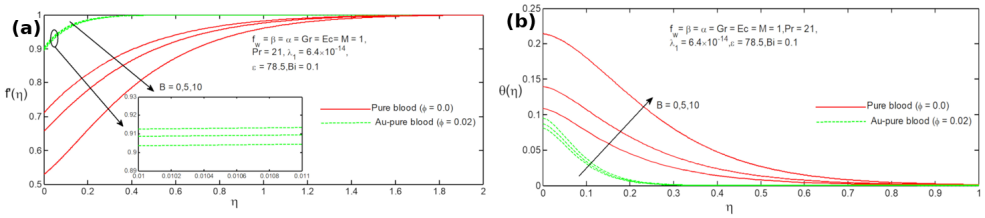

Figure 4. Calculated influence of the ferromagnetic interaction parameter B on (a) the velocity profile $f'(\eta)$ and (b) the temperature profile $\theta(\eta)$. Increasing the dipole effect leads to reduced momentum and elevated temperatures.

As illustrated by the results of Figure 4, the effect of the dipole parameter on the problem under investigation is magneto-thermal coupling rather than mechanical. Specifically, the diminution of $f'(\eta)$ is attributed to greater magnetic resistance to near-wall momentum transfer, whereas increased $\theta(\eta)$ represents enhanced thermal retention or production. Practically, it means that stronger magnetic forcing enhances magnetic targeting, but it also increases thermal loading. Consequently, the permissible operating regime of B should take into account the corresponding thermal response.

The impact of the magnetic field on the problem is described by the magnetic parameter M, which is involved mostly in the Lorentz-force-related and energy aspects of the model. From the results presented in Figure 5, it is clear that higher values of the magnetic parameter lead to amplified dimensionless velocity distributions and diminished temperatures. In the present scaling, such an observation suggests that the velocity field is influenced by a more effective competition between the free-stream recovery term and the magnetic drag term with $(f' - 1)$. The decrease in the temperature distribution, however, implies that the magnetic effect on the velocity profile leads to lower thickness of the thermal layer.

An interesting point about the results presented in Figures 4 and 5 is that the behavior of the profiles differs for B and M. Although M and B represent distinct physical aspects of the same phenomenon, their roles in the transformed equations are different. Specifically, B is directly associated with a localized field gradient and the effect of pyromagnetism, while M is associated with Lorentz resistance and related energy effects. The model therefore separates two magnetic design effects that are sometimes combined too loosely in simplified MHD descriptions.

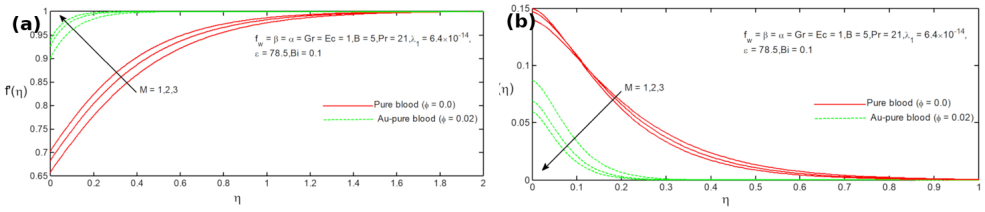

Figure 5. Calculated influence of the magnetic parameter M on (a) the velocity profile $f'(\eta)$ and (b) the temperature profile $\theta(\eta)$.

7.3. Role of buoyancy, convective heat transfer, and viscous dissipation

The role of the Grashof number Gr is the relative magnitude of the buoyant force compared to the stretching force. As depicted in Figure 6, an increasing value of the Grashof number makes the fluid flow faster and reduces the temperature field. The former arises due to the favorable buoyancy assistance to the streamwise velocity, whereas the latter comes from the contraction of the thermal boundary layer. From the mechanical

engineering perspective, buoyancy can be viewed as an internal momentum aid, helping to resist the magnetic deceleration and/or viscosity.

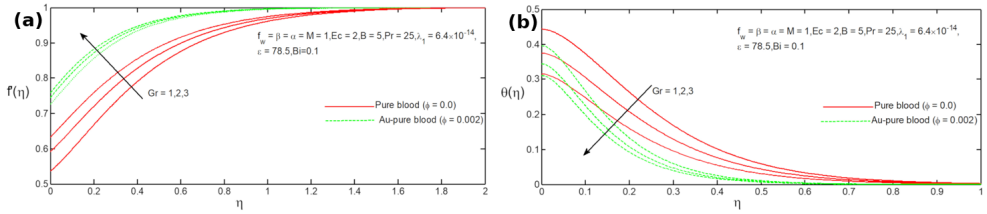

Figure 6. Computed influence of the Grashof number Gr on (a) the velocity profile $f'(\eta)$ and (b) the temperature profile $\theta(\eta)$. With an increase in buoyancy, the thermal boundary layer gets thinner.

Figure 6 demonstrates that heat gradients may influence the mechanical system. The change in Grashof number results not only in a temperature change but also modifies the mechanical part of the model. The acceleration of the flow helps to reach faster the state of free flow, reducing the thermal residence time. Therefore, heat transfer and mechanical properties of a biomagnetic system must be investigated jointly rather than independently.

The influence of the Biot number is shown in Figure 7. As expected, the increase in the Biot number leads to higher heat transfer rates across the channel walls. Therefore, with an increase in Biot number, the temperature field grows significantly. It means that a better thermal contact between the wall and the surrounding fluid results in an increased temperature inside the channel. At the same time, changing the Biot number also influences the mechanics of the flow in the form of modifying the buoyancy factor. From the engineering point of view, the Biot number characterizes the efficiency of the thermal source interaction with the wall. Therefore, it can be considered as a boundary parameter.

Figure 7 demonstrates that wall-side thermal properties still have an impact in cases when the magnetic forces are involved. With a growing Biot number, the temperature at the wall rises since the wall-side thermal boundary condition becomes closer to the temperature of the heating fluid. As a result, the heat flux at the wall is defined by both fluid-side and wall-side thermal gradients.

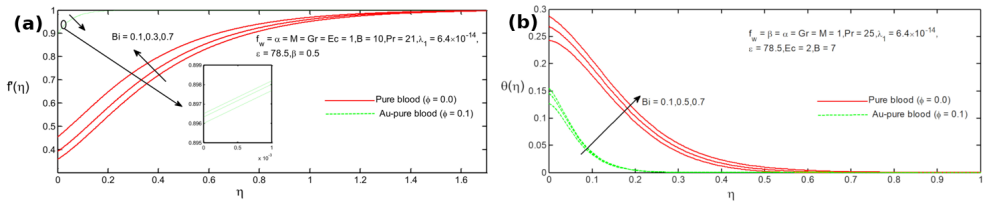

Figure 7. Computed influence of the Biot number Bi on (a) the velocity profile $f'(\eta)$ and (b) the temperature profile $\theta(\eta)$. Wall-side convective heat exchange contributes to the thermal field.

The contribution of the Eckert number comes from the viscous dissipation. As seen in Figure 8, a higher Eckert number results in a significant growth in the temperature profile. Viscous heating causes the conversion of mechanical energy to internal energy. Moreover, it is important at the high values of temperature gradients close to the wall. In the present context, viscous dissipation competes with magnetic heating and convective heat transfer. Therefore, the temperature profile represents the balance between diffusion and mechanical energy transformation in addition to other heat sources [33,34].

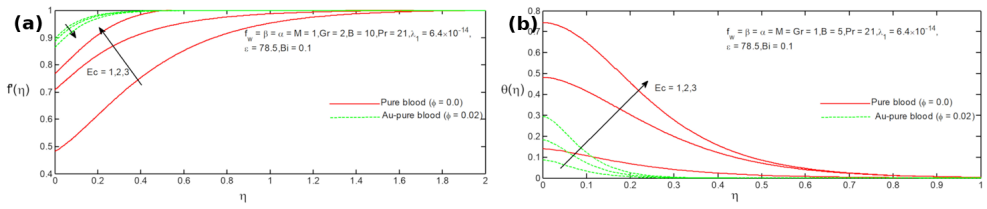

Figure 8. Computed influence of the Eckert number Ec on (a) the velocity profile $f'(\eta)$ and (b) the temperature profile $\theta(\eta)$. An increase in viscous dissipation generates additional heat and increases the thermal boundary layer.

Figure 8 is particularly useful for studying micro-scale flow or flows with high gradients, in which mechanical energy conversion cannot be neglected. With an increase in the Eckert number, the relative weight of imposed temperature difference decreases because of heat generation in the process. Such a situation can be problematic for external cooling in case the magnetic forces prolong the residence time of the flow in the pipe.

7.4. Effect of the Prandtl number

As shown in Figure 9, higher values of the Prandtl number Pr have a positive effect on the velocity profile and decrease the temperature profile. Since the Prandtl number indicates the ratio of the momentum diffusion coefficient to the thermal diffusion coefficient, larger Pr leads to smaller thermal diffusion and thermal boundary layer thickness. These effects are immediate and obvious. The observed rise in the velocity profile is due to the change in the ratio between thermal buoyancy forces and hydrodynamic effects. From the practical standpoint, what should be noted is that thermal diffusivity continues to play the central role in the coupled problem under consideration despite strong coupling.

The interpretation of the results of Figure 9 depends on the considered nanofluid model. Increased value of the Prandtl number reduces thermal diffusion relative to momentum diffusion. Therefore, more thermal energy is localized near the sheet, resulting in increased thermal gradient at the wall. On the other hand, less thermal energy is present in the far-field region. It is thus crucial to have accurate thermal conductivity and heat capacity of the fluid mixture for the estimation of the influence of gold concentration on Pr.

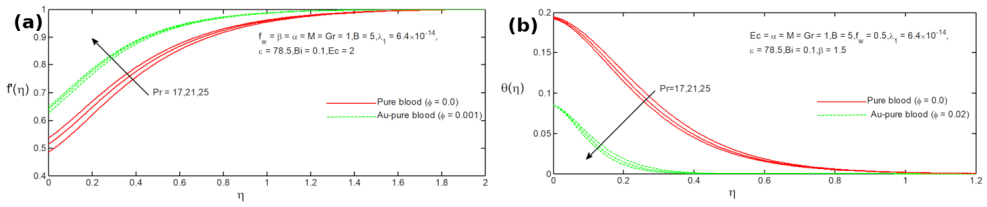

Figure 9. Computed effect of the Prandtl number Pr on (a) the velocity profile $f'(\eta)$ and (b) the temperature profile $\theta(\eta)$. Larger Pr implies reduced heat diffusion and thinner thermal boundary layer.

7.5. Wall transport properties and engineering implications

Global dependencies of the controlling parameters on wall transport are compiled in Table 4 and depicted in Figures 10 and 11. The local Nusselt number responds sharply to the interplay between magnetic forcing, dissipation, buoyancy, suction, and convective heating, since all of these modify the wall thermal gradient either directly or indirectly through the boundary-layer structure. Likewise, the skin-friction coefficient is sensitive to the hydrodynamic slip and suction as well as indirect effects via the boundary-layer structure related to thermal and magnetic fields. The key engineering lesson from these results is that magnetic forcing alone cannot be used to predict wall heat exchange efficiency,

since the actual response of wall quantities is determined by the combination of magnetic forcing with mass and heat transfer at the wall.

Table 4. Qualitative effect of the principal parameters on the velocity field, temperature field, skin friction, and heat-transfer rate in the present biomagnetic Au–blood model.

Increase in parameter	Velocity	Temperature	Skin friction	Heat-transfer rate
Suction, f_w	↑	↓	generally ↑	generally ↑
Slip, β	↑	↓	↓	trend-dependent
Ferromagnetic parameter, B	↓	↑	trend-dependent	trend-dependent
Magnetic parameter, M	↑	↓	trend-dependent	trend-dependent
Grashof number, Gr	↑	↓	trend-dependent	generally ↑
Biot number, Bi	weak change	↑	weak change	trend-dependent
Eckert number, Ec	weak change	↑	weak change	generally ↓
Prandtl number, Pr	↑	↓	generally ↑	generally ↑

The trends obtained in Table 4 represent an engineering-oriented summary. Entries listed as “trend-dependent" do not correspond to unpredictable numerical results, but imply a complex competition between multiple mechanisms of the process under study. For instance, increasing some parameter will lead to the thinning of the boundary layer, but at the same time to the generation of additional thermal energy in the flow, and the resulting wall gradient will depend on the dominant mechanism. This allows for distinguishing controllable wall effects from the complex combinations requiring optimization.

As follows from Figure 10, the wall heat-transfer response to magnetic forcing cannot be generalized in the form of a simple empirical law. Increasing Ec will lead to the addition of thermal energy to the flow, which can reduce its effective heat-removing capability. Meanwhile, suction and favorable buoyancy can produce sharp thermal gradient in spite of thinning the layer thickness. An increased value of B acts in a totally different way, by introducing an internal magnetic field localized near the dipole that modifies both the momentum and thermal parts of the equations. As a result, improving one wall transport property using magnetic forcing will deteriorate another one unless other factors (suction and heating intensity) are considered simultaneously.

A similar conclusion emerges from Figure 11 concerning skin-friction coefficient response, now emphasizing the mechanical aspect of the problem. The behavior of $f''(0)$ as a function of M becomes modified by the thermal diffusivity parameter Pr due to feedback of the temperature field on buoyancy forces, and by the wall slip β. In view of applications involving blood-compatible surfaces, reducing wall shear stress through slip can become preferable, although such action may be accompanied by the corresponding change in wall heat transfer.

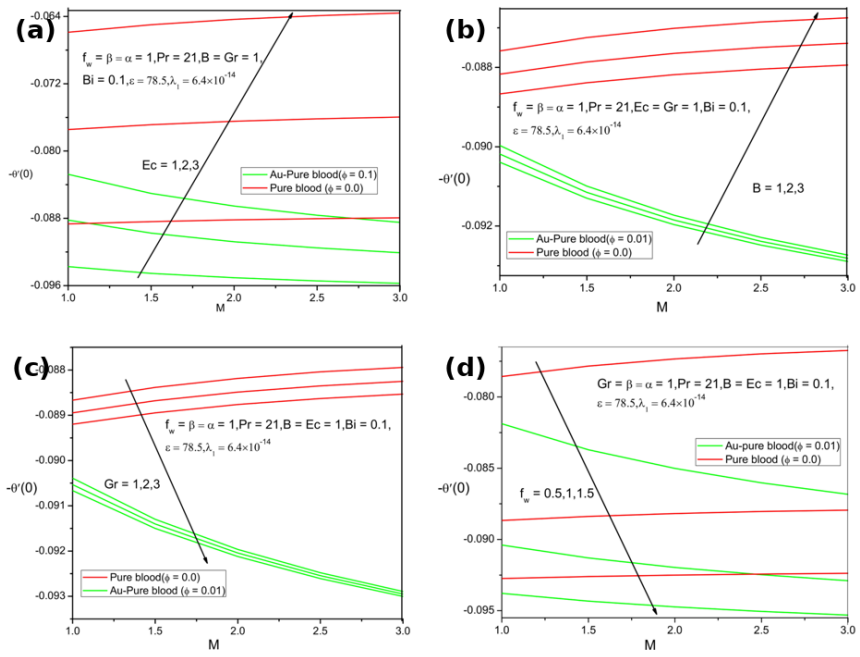

Figure 10. Local Nusselt number $-\theta'(0)$ as a function of the magnetic parameter M for different values of (a) Ec, (b) B, (c) Gr, and (d) f_w.

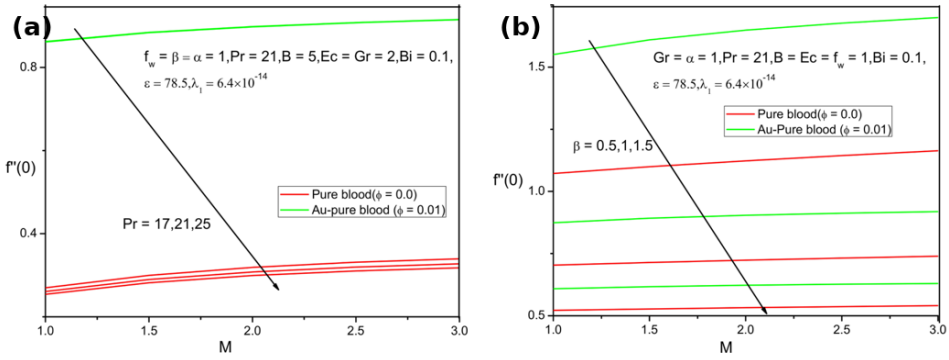

Figure 11. Skin-friction coefficient $f''(0)$ as a function of the magnetic parameter M for different values of (a) Pr and (b) β.

7.6. Numerical benefits of the spectral formulation

In addition to the physical trends discussed above, the study illustrates the computational benefits of spectral discretization in coupled bio-magnetic transport. The partial differential equations have nonlinearities involving first and second order derivatives as well as wall-dependent dipole source terms. Therefore, while a lower-order discretization may be able to capture the general form of the solution, the wall gradients will not converge to the right values. On the other hand, using the Chebyshev collocation scheme means concentrating computational resources near the wall in a context where global polynomial information is known.

It is thus an excellent tool for parametric investigation and continuation with respect to magnetic or wall control parameters. In addition, because the same nodal approximation is utilized to compute the profiles and the wall derivatives, the calculated values of $f''(0)$

and $-\theta'(0)$ are consistent with the computed velocities and temperatures. This consistency will be beneficial in further investigations of non-Newtonian blood flow, thermal radiation effects, porous media, magnetic permeability variation, and particle reactions.

8. Conclusions

In summary, a two-phase boundary-layer model of biomagnetic Au–blood nanofluid flow induced by a permeable linearly stretching sheet under action of local magnetic dipole, velocity slip, suction, convection, mixed convection, viscous dissipation, and Joule magnetic forcing effects has been analyzed. In particular, the governing equations have been reduced to a set of nonlinear ODEs and numerically solved using the spectral collocation technique in the form of Chebyshev polynomials on Gauss–Lobatto nodes. This method was chosen due to its superior stability and ability to accurately approximate derivative values near the boundaries, which are essential in estimating key engineering quantities such as wall shear stress and local heat transfer coefficient.

This study shows that suction represents one of the strongest mechanisms of compressing the hydrodynamic and thermal boundary layer thicknesses, leading to a higher gradient in the wall vicinity and hence enhancing skin friction and local Nusselt number. Velocity slip, on the other hand, represents a distinct mechanism through which the boundary layer is compressed, affecting the near-wall regime of flow and heat exchange by relaxing the shear stress. Thus, suction and slip mechanisms cannot be conflated into a single wall-control method since they affect the flow and heat transfer in fundamentally different ways.

Concerning magnetic effects, this study highlights a difference between dipole-gradient and Lorentz forcing types. Namely, an increase in the parameter of ferromagnetic interaction B leads to a slower flow, resulting in a rise in the temperature distribution due to higher retention. However, an increase in the magnetic parameter M, which represents Lorentz force, leads to a more complex response, depending on the balance between the free stream pressure, magnetic field resistance, and joules heat generation. This aspect has implications for biomedical applications in that a stronger dipole magnetic actuation can potentially lead to better manipulation of fluids, while adding to their heat load.

Finally, it has been shown that thermal parameters control the solution to a high degree. An increase in the biot number Bi leads to a higher temperature level due to greater heat input into the domain. At the same time, a higher Eckert number Ec means that more energy is lost to the temperature field due to viscous dissipation. Further, an increase in the Prandtl number Pr leads to thinner thermal boundary layer due to weaker thermal diffusion. Lastly, Gr parameter promotes streamwise motion and indirectly results in thermal compression. Hence, the rate of wall heat transfer is subject to competitive forces of wall heating, dissipation, buoyancy, suction, and magnetic actuation.

Based on this analysis, it can be inferred that skin friction and local heat transfer cannot be estimated with a single parameter since those which lead to the contraction of boundary layers tend to produce higher wall gradients, while those that heat the flow tend to weaken wall gradients. As such, a trend matrix and plots of the wall responses represent a convenient means of interpreting the data, and magnetic actuation should be combined with wall suction, slip, and heat exchange conditions.

To conclude, a numerical framework for analyzing the effects of magnetic actuation on Au–blood nanofluids' flow and heat transfer near permeable surfaces has been developed. This study can be extended by including dependence of blood viscosity on shear rate, nanoparticle migration, pulsatile stretch, interaction with tissue, radiation, and measured magnetic-field distribution.

Nomenclature

a	stretching constant
B	ferromagnetic interaction parameter
B_0	applied magnetic-field strength
Bi	Biot number
C_f	skin-friction coefficient
C_p	specific heat at constant pressure
d	dipole distance from the sheet
Ec	Eckert number
f	dimensionless stream-function function
f_w	suction parameter
g	gravitational acceleration
Gr	Grashof number
H	magnetic-field intensity
h_f	wall heat-transfer coefficient
k	thermal conductivity
K	pyromagnetic coefficient
M	magnetic parameter
Nu_x	local Nusselt number
Pr	Prandtl number
q_w	wall heat flux
Re_x	local Reynolds number
T	fluid temperature
T_f	heating-fluid temperature
T_∞	ambient temperature
u, v	velocity components in the x- and y-directions
U_∞	stretching-sheet or external velocity scale
V_w	wall mass-transfer velocity
x, y	Cartesian coordinates
α	dimensionless dipole distance
β	slip parameter or thermal expansion coefficient (context dependent)
ε	Curie-temperature parameter
η	similarity variable
θ	dimensionless temperature
λ	slip coefficient
λ_1	viscous-dissipation constant
μ	dynamic viscosity
μ_0	magnetic permeability of free space
ν_f	kinematic viscosity of the base fluid
ρ	density
σ	electrical conductivity
ϕ	nanoparticle volume fraction

References

[1] Tzirtzilakis, E. E. (2005). A mathematical model for blood flow in magnetic field. *Physics of Fluids*, 17(7), 077103.

[2] Pennes, H. H. (1948). Analysis of tissue and arterial blood temperatures in the resting human forearm. *Journal of Applied Physiology*, 1(2), 93–122.

[3] Schlichting, H., & Gersten, K. (2000). *Boundary-Layer Theory* (8th ed.). Berlin: Springer.

[4] Rosensweig, R. E. (1985). *Ferrohydrodynamics*. Cambridge: Cambridge University Press.

[5] Kafoussias, N. G., & Tzirtzilakis, E. E. (2003). Biomagnetic fluid flow over a stretching sheet with non-linear temperature dependent magnetization. *Zeitschrift fuer angewandte Mathematik und Physik*, 54, 551–565.

[6] Choi, S. U. S. (1995). Enhancing thermal conductivity of fluids with nanoparticles. In *Developments and Applications of Non-Newtonian Flows*, ASME FED-Vol. 231/MD-Vol. 66, 99–105.

[7] Buongiorno, J. (2006). Convective transport in nanofluids. *Journal of Heat Transfer*, 128(3), 240–250.

[8] Eastman, J. A., Choi, S. U. S., Li, S., Yu, W., & Thompson, L. J. (2001). Anomalously increased effective thermal conductivities of ethylene glycol-based nanofluids containing copper nanoparticles. *Applied Physics Letters*, 78(6), 718–720.

[9] Jain, P. K., Huang, X., El-Sayed, I. H., & El-Sayed, M. A. (2008). Noble metals on the nanoscale: optical and photothermal properties and some applications in imaging, sensing, biology, and medicine. *Accounts of Chemical Research*, 41(12), 1578–1586.

[10] Dreaden, E. C., Alkilany, A. M., Huang, X., Murphy, C. J., & El-Sayed, M. A. (2012). The golden age: gold nanoparticles for biomedicine. *Chemical Society Reviews*, 41(7), 2740–2779.

[11] Hu, X., Zhang, Y., Ding, T., Liu, J., & Zhao, H. (2020). Multifunctional gold nanoparticles: a novel nanomaterial for various medical applications and biological activities. *Frontiers in Bioengineering and Biotechnology*, 8, 990.

[12] Crane, L. J. (1970). Flow past a stretching plate. *Zeitschrift fuer angewandte Mathematik und Physik*, 21(4), 645–647.

[13] Gupta, P. S., & Gupta, A. S. (1977). Heat and mass transfer on a stretching sheet with suction or blowing. *Canadian Journal of Chemical Engineering*, 55(6), 744–746.

[14] Wang, C. Y. (2002). Flow due to a stretching boundary with partial slip–an exact solution of the Navier–Stokes equations. *Chemical Engineering Scie nce*, 57(17), 3745–3747.

[15] Andersson, H. I. (2002). Slip flow past a stretching surface. *Acta Mechanica*, 158(1–2), 121–125.

[16] Aziz, A. (2009). A similarity solution for laminar thermal boundary layer over a flat plate with a convective surface boundary condition. *Communications in Nonlinear Science and Numerical Simulation*, 14(4), 1064–1068.

[17] Makinde, O. D., & Aziz, A. (2011). Boundary layer flow of a nanofluid past a stretching sheet with a convective boundary condition. *International Journal of Thermal Sciences*, 50(7), 1326–1332.

[18] Khanafer, K., Vafai, K., & Lightstone, M. (2003). Buoyancy-driven heat transfer enhancement in a two-dimensional enclosure utilizing nanofluids. *International Journal of Heat and Mass Transfer*, 46(19), 3639–3653.

[19] Khan, W. A., & Pop, I. (2010). Boundary-layer flow of a nanofluid past a stretching sheet. *International Journal of Heat and Mass Transfer*, 53(11–12), 2477–2483.

[20] Kuznetsov, A. V., & Nield, D. A. (2010). Natural convective boundary-layer flow of a nanofluid past a vertical plate. *International Journal of Thermal Sciences*, 49(2), 243–247.

[21] Trefethen, L. N. (2000). *Spectral Methods in MATLAB*. Philadelphia: Society for Industrial and Applied Mathematics.

[22] Canuto, C., Hussaini, M. Y., Quarteroni, A., & Zang, T. A. (2006). *Spectral Methods: Fundamentals in Single Domains*. Berlin: Springer.

[23] Boyd, J. P. (2001). *Chebyshev and Fourier Spectral Methods* (2nd ed.). Mineola, NY: Dover Publications.

[24] Tzirtzilakis, E. E. (2015). Biomagnetic fluid flow in an aneurysm using ferrohydrodynamics principles. *Physics of Fluids*, 27(6), 061902.

[25] Brinkman, H. C. (1952). The viscosity of concentrated suspensions and solutions. *Journal of Chemical Physics*, 20(4), 571.

[26] Maxwell, J. C. (1881). *A Treatise on Electricity and Magnetism* (2nd ed.). Oxford: Clarendon Press.

[27] Hamilton, R. L., & Crosser, O. K. (1962). Thermal conductivity of heterogeneous two-component systems. *Industrial and Engineering Chemistry Fundamentals*, 1(3), 187–191.

[28] Gabriel, S., Lau, R. W., & Gabriel, C. (1996). The dielectric properties of biological tissues: III. Parametric models for the dielectric spectrum of tissues. *Physics in Medicine and Biology*, 41(11), 2271–2293.

[29] Hinghofer-Szalkay, H. (1985). Volume and density changes of biological fluids with temperature. *Journal of Applied Physiology*, 59(6), 1686–1689.

[30] Haynes, W. M. (Ed.). (2016). *CRC Handbook of Chemistry and Physics* (97th ed.). Boca Raton, FL: CRC Press.

[31] Daniel, Y. S. (2016). Steady MHD boundary-layer slip flow and heat transfer of nanofluid over a convectively heated nonlinear permeable sheet. *Journal of Advanced Mechanical Engineering*, 3(1), 1–14.

[32] Tzirtzilakis, E. E., & Tanoudis, G. B. (2003). Numerical study of biomagnetic fluid flow over a stretching sheet with heat transfer. *International Journal of Numerical Methods for Heat and Fluid Flow*, 13(7), 830–848.

[33] Cortell, R. (2007). Viscous flow and heat transfer over a nonlinearly stretching sheet. *Applied Mathematics and Computation*, 184(2), 864–873.

[34] Oztop, H. F., & Abu-Nada, E. (2008). Numerical study of natural convection in partially heated rectangular enclosures filled with nanofluids. *International Journal of Heat and Fluid Flow*, 29(5), 1326–1336.